

# Diversity and wiring variability of olfactory local interneurons in the *Drosophila* antennal lobe

Ya-Hui Chou<sup>1,3</sup>, Maria L Spletter<sup>1,3</sup>, Emre Yaksi<sup>2,3</sup>, Jonathan C S Leong<sup>1</sup>, Rachel I Wilson<sup>2</sup> & Liqun Luo<sup>1</sup>

**Local interneurons are essential in information processing by neural circuits. Here we present a comprehensive genetic, anatomical and electrophysiological analysis of local interneurons (LN)s in the *Drosophila melanogaster* antennal lobe, the first olfactory processing center in the brain. We found LNs to be diverse in their neurotransmitter profiles, connectivity and physiological properties. Analysis of >1,500 individual LNs revealed principal morphological classes characterized by coarsely stereotyped glomerular innervation patterns. Some of these morphological classes showed distinct physiological properties. However, the finer-scale connectivity of an individual LN varied considerably across brains, and there was notable physiological variability within each morphological or genetic class. Finally, LN innervation required interaction with olfactory receptor neurons during development, and some individual variability also likely reflected LN–LN interactions. Our results reveal an unexpected degree of complexity and individual variation in an invertebrate neural circuit, a result that creates challenges for solving the *Drosophila* connectome.**

Neurons can be divided into two general categories: projection neurons, whose axons connect discrete regions of neural tissue, and local interneurons, whose processes are restricted to a single region. Local interneurons are important in neural computation. For example, horizontal and amacrine cells in the vertebrate retina are instrumental in transforming incoming signals from photoreceptors, such that information regarding contrast, motion and color can be encoded by retinal ganglion cells and transmitted into the brain. Every vertebrate brain region contains many local interneuron types, as defined by morphology, histological markers and physiology. Different types are thought to have distinct functions<sup>1</sup>. However, it is less clear whether the same kind of diversity exists in simpler organisms such as *Drosophila*. Systematic identification and characterization of local interneurons is a prerequisite to understanding how nervous systems process information<sup>2</sup>.

The fly antennal lobe is an attractive model neural circuit because of its elegant anatomical and functional organization and its genetic tractability. All olfactory receptor neurons (ORNs) that express the same odorant receptor project their axons to the same antennal lobe glomerulus, and most antennal lobe projection neurons (PNs) send dendrites into a single glomerulus to receive direct input from one ORN class<sup>3</sup>. Genetic access is available to many classes of ORNs and PNs<sup>3</sup>. In contrast to these input and output neurons, LNs in the fly antennal lobe are much less well characterized.

In the olfactory bulb, the vertebrate analog of the antennal lobe, there are ~100 local interneurons for each projection neuron<sup>4</sup>, one of the highest local interneuron/projection neuron ratios in any mammalian brain region. Olfactory bulb interneurons are morphologically diverse and are hypothesized to be important in gain control,

spike synchronization and decorrelation of the representations of similar odorants<sup>4–6</sup>. Studies of antennal lobe LNs in larger insects have described a variety of LN morphologies<sup>7–11</sup>. In comparison, the limited data available suggested that *Drosophila* antennal lobe LN have relatively simple morphologies, with each LN innervating all glomeruli, although LN that are not pangolesmolar have been described in more recent studies<sup>12–18</sup>. Understanding how ORN input is transformed into PN output by the antennal lobe requires a deeper understanding of antennal lobe LN.

Here we took a systematic approach to identifying and characterizing LN in the *Drosophila* antennal lobe. Using specific Gal4 lines in conjunction with the MARCM (mosaic analysis with repressible cell marker) method<sup>19</sup> and dye fills, we analyzed the morphology of >1,500 LN at the single-cell level. This analysis revealed a remarkable diversity of glomerular innervation patterns, which can be used to define distinct morphological classes of LN. Main morphological LN classes have distinctive electrophysiological properties that help define their potential functions within the circuit. At a fine scale, our analysis also demonstrated that the innervation pattern of an individual LN varied across brains. Similarly, even within a morphologically or genetically defined class of LNs, we found considerable variability in physiological properties. This individual variation may in part reflect the role of cell–cell interactions during development. Our findings imply that LN play unexpectedly diverse roles in olfactory processing in the fly antennal lobe. The wiring variability of LN suggests that the wiring diagram differs considerably between individual fly brains, and that individual variations in behavior may in part reflect these kinds of fine-scale variations at the cellular level.

<sup>1</sup>Howard Hughes Medical Institute, Department of Biology, Stanford University, Stanford, California, USA. <sup>2</sup>Department of Neurobiology, Harvard Medical School, Boston, Massachusetts, USA. <sup>3</sup>These authors contributed equally to this work. Correspondence should be addressed to L.L. (lluo@stanford.edu) or R.I.W. (rachel\_wilson@hms.harvard.edu).

Received 28 September 2009; accepted 22 December 2009; published online 7 February 2010; doi:10.1038/nn.2489

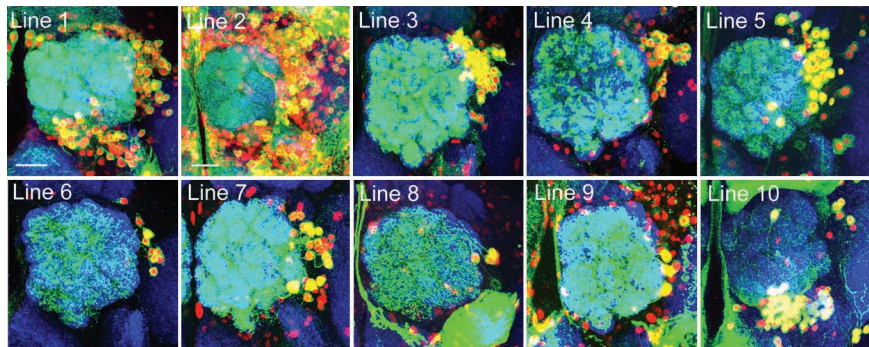


**Figure 1** Antennal lobe LNs. Expression patterns of the ten Gal4 lines used in this study. Green, Gal4-driven mCD8-GFP; red, Gal4-driven nuclear  $\beta$ -galactosidase or nuclear RFP; blue, neuropil staining by monoclonal antibody nc82, specific for a neuropil marker. Scale bars, 20  $\mu$ m. (Scale is the same for lines 1 and 3–10.)

## RESULTS

### Antennal lobe LNs and their neurotransmitter profiles

We used ten Gal4 lines to genetically access antennal lobe LNs. The expression patterns of these lines span a range from hundreds of neurons near the antennal lobe to just a handful of LNs (Fig. 1). For simplicity, we refer to these Gal4 lines as lines 1–10 (see Online Methods). In addition to LNs—which we defined as neurons whose cell bodies were near the antennal lobe and whose processes were restricted to the antennal lobes—several lines also labeled ORNs, PNs and/or neurons near the antennal lobe that project to other areas of the brain (Supplementary Fig. 1).

LN cell bodies are located in two clusters: a large but continuous cluster lateral and dorsolateral to the antennal lobe, which included most LNs labeled by lines 1 and 3–9, and a separate cluster ventral to the antennal lobe, which included most LNs labeled by line 10 (Fig. 1 and Supplementary Fig. 1). To determine the number and the potential overlap of LNs labeled by these Gal4 lines, we counted the numbers of nuclei labeled by nuclear markers driven from individual Gal4s, as well as from their combinations in the same fly (Supplementary Table 1). These data suggested that some lines label largely nonoverlapping LN populations, whereas other lines overlap partly or completely.

Line 5 seems to include all cells that were labeled by lines 6–9. All ~56 cells labeled by line 5 are LNs because (i) line 5–driven membrane marker mCD8-GFP did not label any neurons that send processes out of the antennal lobe (Fig. 1), and (ii) the entire arborizations of all 578 single cells from systematic MARCM analysis and biocytin fill (see below) from line 5 were within the antennal lobe. On the basis of the total number of LNs labeled by lines 3, 4 and 5 in the same fly (Supplementary Table 1) and cell body positions from neuroblast clone analysis (Supplementary Fig. 1), we estimate that there were ~100 LNs labeled by lines 1 and 3–9, which are mostly ipsilaterally projecting LNs in the lateral cluster (see below). Line 10 labeled mostly bilaterally projecting LNs (see below) in the ventral cluster. Therefore, the lower bound for *Drosophila* LNs (labeled by our Gal4 lines) is ~100 ipsilaterally projecting and ~100 bilaterally projecting LNs for each antennal lobe.

Although LNs are traditionally considered to be inhibitory neurons that release GABA as their neurotransmitter, recent studies have suggested that some LNs can be excitatory<sup>14,20</sup> and cholinergic<sup>14,17</sup>. We examined the neurotransmitter type of different Gal4 lines by double staining with antibodies to GABA and choline acetyltransferase. Antibody specificity was validated by loss of staining in MARCM clones homozygous for a null mutation of *Glutamic acid decarboxylase-1*

or *Choline acetyltransferase* (Supplementary Fig. 2). Most LNs were GABAergic; however, there were a few cholinergic cells, and a larger minority that were neither GABAergic nor cholinergic (Supplementary Table 1 and Supplementary Fig. 2). Staining for other neurotransmitter types identified a few dopaminergic and many (mostly ventral) glutamatergic LNs (Supplementary Fig. 3). These results indicate that although most LNs are GABAergic, some LNs use different neurotransmitters or their combinations, emphasizing the potential diversity in the functional roles of different LNs.

### Morphological diversity of LNs

The MARCM method can be used to label single neurons born at specific developmental times<sup>21,22</sup>. We performed systematic MARCM labeling of LNs from these ten Gal4 lines throughout development. Figure 2 shows representative images from 1,439 single-cell LN clones. The LNs showed substantial morphological diversity.

We identified five broad categories of ipsilaterally projecting LNs on the basis of the extent of their arborization in the antennal lobe: the entire antennal lobe (panglomerular; Fig. 2a), all but a few glomeruli (Fig. 2b), a continuous region of the antennal lobe (Fig. 2c), discontinuous or patchy regions of the antennal lobe (Fig. 2d) and 1–3 glomeruli (oligoglomerular; Fig. 2e). Within each category, however, there was considerable diversity. For example, although many LNs arborized nearly the entire antennal lobe, they differed in the density of arborization and the thickness of their processes (Fig. 2a,b and Supplementary Fig. 4). For LNs that skip a few glomeruli or arborize in a continuous region, different individuals skipped different glomeruli or arborized in different regions of the antennal lobe (Fig. 2b,c and Supplementary Fig. 5). Finally, bilaterally projecting LNs showed heterogeneous ipsilateral and contralateral arborization patterns (Fig. 2f).

### Subcellular distribution of presynaptic terminals in LNs

All neurotransmitter release of LNs occurs within the antennal lobe, but does each LN releases neurotransmitter throughout its arbor, or only in a restricted zone? To examine how presynaptic terminals are distributed within individual LNs, we performed a large subset of MARCM single-cell labeling with an additional synaptotagmin-hemagglutinin (HA) marker, which labels presynaptic terminals<sup>23</sup>. In general, synaptotagmin-HA labeled puncta throughout an LN's processes (Fig. 2 and Supplementary Fig. 4). These data suggest that, as a general rule, LNs broadcast transmitter release across their arborization without notable glomerular selectivity.

However, in exception to the above rule, some oligoglomerular and bilateral LNs had a more selective synaptotagmin-HA distribution (Fig. 2e,f and Supplementary Fig. 4). These LNs therefore seem to deliver information to only a subset of the glomeruli they innervate.

### Statistical analysis of glomerular innervation patterns

Given the diversity of morphologies, we next analyzed these data systematically with the aim of identifying organizational principles of the LN network. An important feature of an LN is its glomerular innervation pattern, as this determines which olfactory channels the LN may receive information from and send information to. We therefore started by analyzing the glomerular innervation patterns of individual LNs (Fig. 3).

We scored 1,532 individual LNs (1,439 from MARCM single-cell clones; 93 from dye fills during whole-cell patch-clamp recording) for their innervation of 54 glomeruli in the antennal lobe (Fig. 3b and Supplementary Tables 2 and 3). We used hierarchical clustering

to organize the 1,532 LNs according to their binary ipsilateral glomerular innervation patterns. This analysis revealed several distinct morphological classes (Fig. 3a). For example, neurons within subcluster C tended to avoid certain glomeruli innervated by trichoid

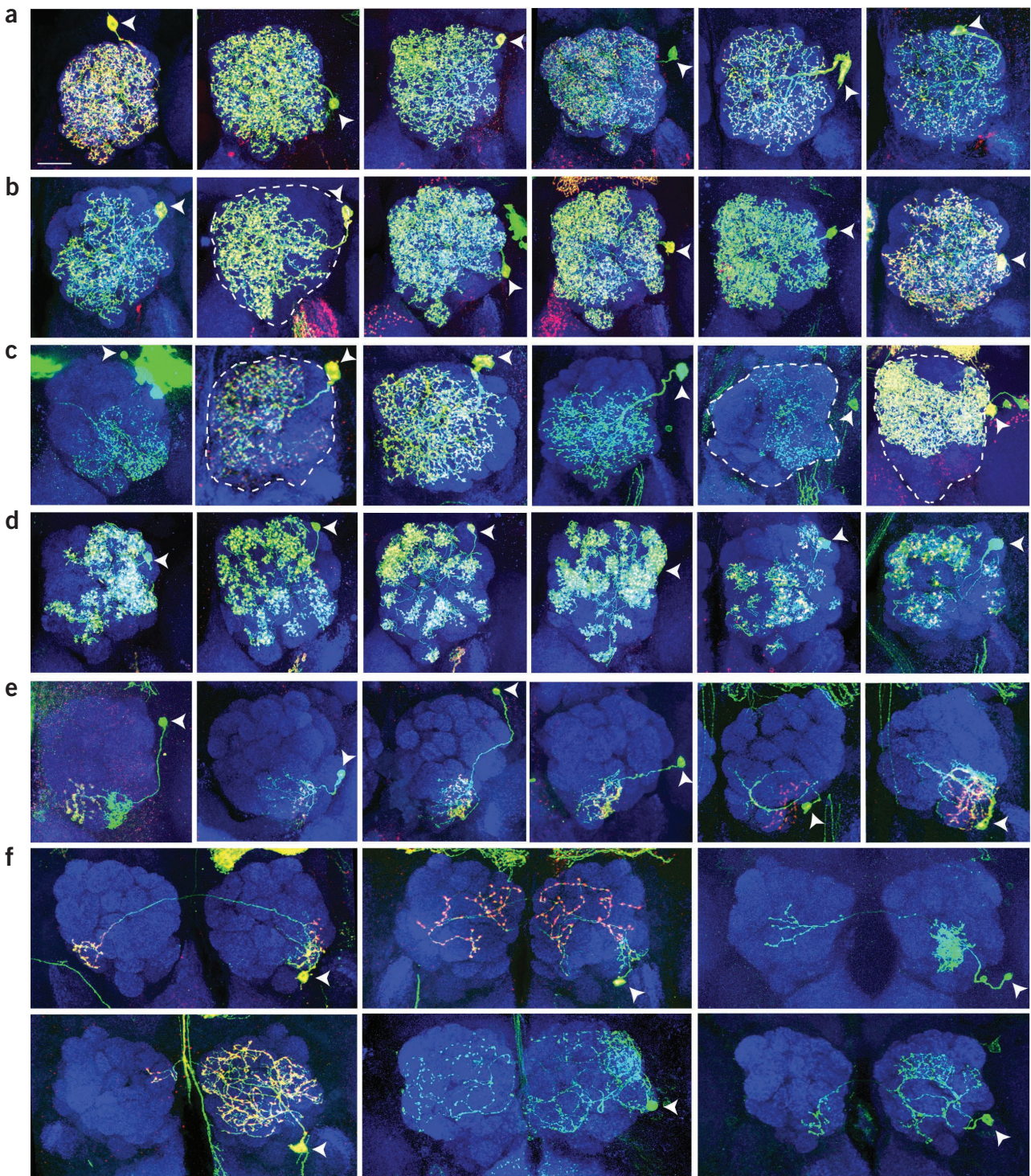
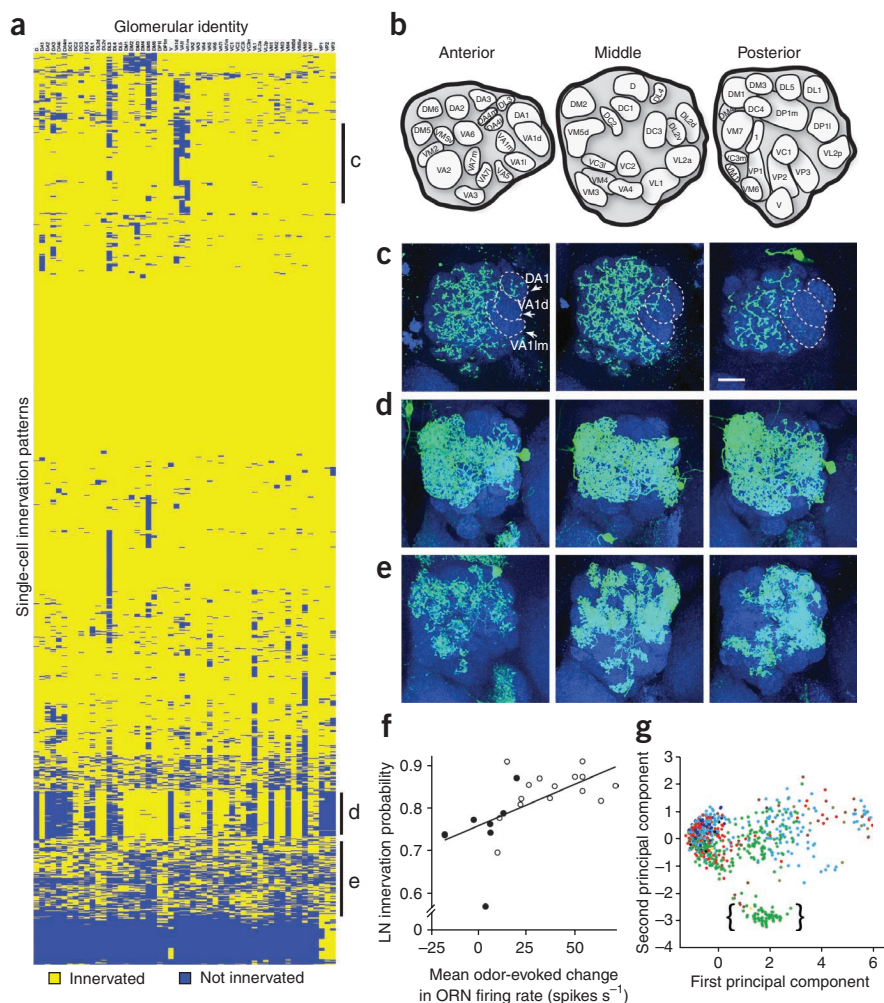


**Figure 2** Diversity of LN morphology. (a–e) Representative arborization patterns of single-cell MARCM clones of ipsilaterally projecting LNs. Each row presents examples from categories of LNs that innervate all glomeruli (a), all but a few glomeruli (b), continuous (c) or patchy (d) regions of the antennal lobe, and a few glomeruli (e). (f) Representative arborization patterns of bilaterally projecting LNs. Green, mCD8-GFP, labeling LN processes; red, synaptotagmin-HA, a marker for presynaptic terminals; blue, nc82 or N-cadherin staining, highlighting glomerular structures. Some images in c (left and fourth and fifth from left) and f (third, fifth and sixth from top left) do not include synaptotagmin-HA staining. Arrowheads, cell bodies; dashed lines, outline of the antennal lobe. Scale bar, 20  $\mu$ m. Information about corresponding Gal4 lines in this and subsequent figures can be found in Supplementary Table 4.

**Figure 3** Statistical analysis of glomerular innervation patterns. (a) Binary glomerular innervation patterns of 1,532 singly labeled LNs organized by hierarchical clustering. Rows represent innervation patterns of individual cells; columns represent 54 glomeruli. 1,489 were ipsilateral projecting LNs. Of the 43 bilaterally projecting LNs, only the ipsilateral patterns were included in the clustering analysis. Yellow, glomeruli innervated; blue, glomeruli not innervated. (b) Antennal lobe model. The 54 glomeruli we scored for this study are outlined in three sections of the antennal lobe from anterior to posterior. This model is modified after a number of sources<sup>3,43</sup> and derived from tracing nc82-stained brains. (c–e) Three representative images from three selected regions of the LN cluster diagram indicated on the right side in a. Green, mCD8-GFP staining; blue, nc82 or N-cadherin staining. Dashed lines in c mark pheromonal glomeruli DA1, VA1d and VA1l/m. Scale bar, 20  $\mu$ m. (f) The LN innervation probability of a glomerulus correlated positively with the mean odor-evoked firing rate of the ORNs presynaptic to that glomerulus ( $r = 0.63$ ,  $P < 0.005$ ,  $n = 23$  glomeruli). ORN data from ref. 25. Firing rates averaged across 110 odors. Filled symbols represent trichoid glomeruli. (g) Principal component analysis of LN glomerular innervation patterns. In the second dimension, the dumbbell subclass of LNs (bracket) distinctly separates from all other cell types. LNs labeled by different Gal4 lines are marked with different colors. See Supplementary Figure 8 for color code of Gal4 lines and histograms of cell distributions in PC1 and PC2.



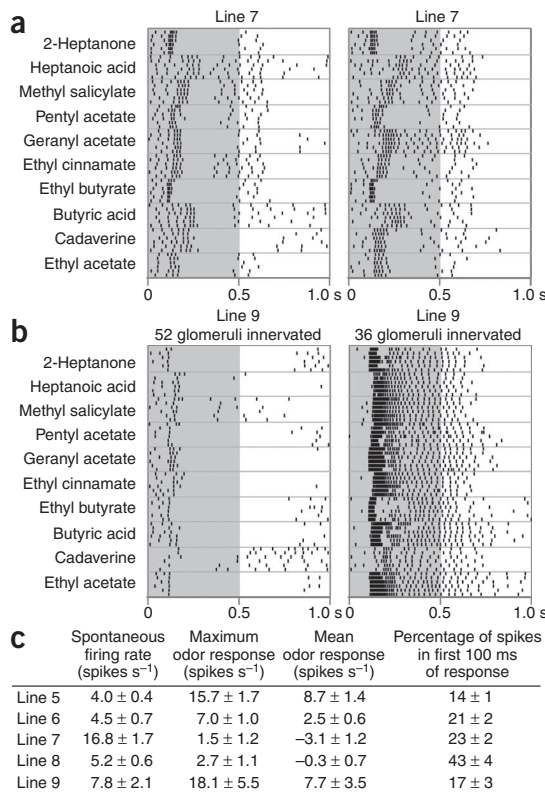
ORN classes that sense pheromones<sup>24</sup> (Fig. 3c). Neurons within subcluster D innervated the central antennal lobe and skipped the dorsal and ventral glomeruli; we call these neurons dumbbell cells, after their shape (Fig. 3d). Neurons within subcluster E showed patchy innervation (Fig. 3e).

Clustering all cells labeled by the same Gal4 (Supplementary Fig. 6) revealed that some Gal4 lines labeled a relatively uniform morphological population of cells (for example, lines 6–8), whereas others labeled a more heterogeneous group (for example, lines 1, 2, 3 and 5). This suggests that some Gal4 lines predominantly label LNs belonging to just a few functional classes, whereas others label a functionally heterogeneous population. We will examine this idea in more detail using electrophysiological recordings (see below).

Clustering all GABA<sup>+</sup> versus GABA<sup>-</sup> cells from our collection revealed that both subtypes included a diversity of morphological patterns (Supplementary Fig. 7). Because most LNs are GABAergic, we considered the hypothesis that LN innervation might be denser in glomeruli that receive more ORN input. We estimated the average lifetime activity of each ORN type using a published data set<sup>25</sup> by averaging the responses of each ORN type across 110 odor stimuli. We found a significant positive correlation between LN innervation probability and mean odor-evoked ORN firing rate (Fig. 3f). This would be consistent with the idea that the density of inhibitory innervation is adapted to the average level of afferent input to each glomerulus<sup>26</sup>, assuming that these stimuli are representative of natural odors.

In addition to hierarchical clustering, we used principal component analysis to identify emergent relationships in the glomerular innervation data set without applying any arbitrary threshold of significance. The first and second principal components (PC1 and PC2; Fig. 3g and Supplementary Fig. 8) for the entire set of innervation patterns accounted for 40% and 10% of the variance in the data, respectively, but 13 additional principal components were needed to account for 25% more. The high number of dimensions necessary to account for variance indicates that innervation patterns are not well described as the linear combination of any small number of basic glomerular relationships. PC1 was essentially a proxy for the number of glomeruli innervated (correlation coefficient 0.9993). Thus, a defining feature of an LN's innervation pattern is the number of glomeruli it connects to. LNs were bimodally distributed on PC2, with a distinctive subcluster containing mainly dumbbell cells (Fig. 3d), confirming that the dumbbell cells constitute a distinctive morphological class.

Next, we considered the LNs that arborize bilaterally. We compared ipsilateral innervation patterns (Supplementary Fig. 9) with corresponding contralateral innervation patterns (Supplementary Fig. 9). We found that many bilateral LNs had symmetric glomerular innervation patterns and overall, ipsi- and contralateral patterns were significantly correlated (Pearson's correlation coefficient  $r = 0.46 \pm 0.05$  (s.e.m.),  $P < 0.01$ ,  $n = 38$ ; Supplementary Fig. 9). In general, the exceptions were LNs with nearly panglomerular ipsilateral innervation.



Finally, on the basis of clustering, we identified a minimal number of LN classes with identifiable innervation patterns and further investigated birth timing and Gal4 expression for those cell types (**Supplementary Fig. 5** and **Supplementary Table 2**). We found that some (although not all) morphological types of LNs were labeled by only a few Gal4 lines and were born in limited time windows. Together, these analyses indicate that LNs are composed of genetically distinct groups of cells defined by a combination of morphology, birth timing and Gal4 expression.

#### Diversity and stereotypy of physiological properties

Do LN genetic categories (Gal4 lines) and morphological categories (glomerular innervation patterns) correlate with physiological properties? To address this, we selected five Gal4 lines that label relatively small subsets of LNs (lines 5–9) and made whole-cell patch-clamp recordings from GFP-labeled somata in each line. We recorded the responses of each cell to a panel of diverse odors (see Online Methods) and filled each cell with biocytin using the patch pipette for visualization after recording. We successfully filled and scored the innervation patterns of 93 LNs.

All these LNs fired spontaneous action potentials, and their spiking was always modulated by odors. LN odor responses were notably diverse and typically varied more across cells than across odors within a cell (**Fig. 4a,b**). Some LNs recorded in the same Gal4 line responded to odors in a similar manner (**Fig. 4a**). For example, the LNs we recorded in line 7 were relatively stereotyped in their functional properties, as were line 8 LNs. In other cases, a Gal4 line could label LNs having very different response profiles (**Fig. 4b**). Line 5 and line 9 were particularly diverse in this respect.

In all these LNs, we measured spontaneous firing rate, mean odor response and maximum odor response. To quantify the time course of the odor response, we also measured the percentage of spikes fired during the first 100 ms of the odor response. All four of these properties were significantly dependent on Gal4 line (**Fig. 4c**). This implies

**Figure 4** Functional stereotypy and diversity among genetic classes.

(a) Rasters showing the similar spiking responses of two line 7 LNs. These LNs are typical of line 7 in having high spontaneous firing rates, weak odor-evoked excitation and strong odor-evoked inhibition. Gray box, the nominal odor stimulus period; there is a delay of about 100 ms before odor reaches the fly. (b) Dissimilar responses of two line 9 LNs. The first of these innervated almost all glomeruli (52 of 54) and was mainly inhibited by all odors, whereas the second innervated a smaller subset of glomeruli and was excited by all odors. Overall, line 9 LNs were diverse. (c) Functional properties of lines 5–9 (mean ± s.e.m.). All these properties were significantly dependent on the Gal4 line of the recorded LN (one-way ANOVA,  $P < 0.0001$ ). For each property, *post hoc* Tukey's tests yielded significant differences ( $P < 0.05$ ) between some but not all of the ten pair-wise comparisons between Gal4 lines. Odor-evoked firing rates are expressed as a change from the spontaneous firing rate.

that differences in Gal4 expression reflect physiological differences between LNs, in spite of the variability within each Gal4 line and the partial overlap in the cells that are labeled by these lines.

#### Physiological differences between morphological classes

Next, we asked whether LN physiological properties were correlated with their morphological class. Because the principal axis for morphological variation was the number of glomeruli each LN innervates (**Fig. 3g**), we began by asking whether any response properties were correlated with this axis. Unexpectedly, LNs that innervate many glomeruli had lower odor-evoked firing rates than LNs that innervate fewer glomeruli. The number of glomeruli innervated by an LN was significantly (although weakly) anticorrelated with the average strength of its odor responses (Pearson's  $r = -0.2$ ,  $P < 0.05$ ).

This finding motivated us to examine the physiology of panglomerular LNs in particular because these cells innervate the largest number of glomeruli. This class comprised 28% of the cells from which we recorded. On average, panglomerular LNs had significantly higher spontaneous firing rates than other LNs (**Fig. 5a**). In the presence of an odor, spontaneous spiking in many panglomerular cells shut down completely, sometimes after a brief burst at odor onset, whereas others modestly increased their firing rate in the presence of odors (**Fig. 5b**). Overall, odor-evoked changes in firing rate were significantly weaker in panglomerular cells than in other LNs (**Fig. 5a**).

A second main class of LNs that we recorded from were LNs that selectively avoided glomerulus VA1d and frequently also avoided DL3 (**Fig. 3c**). These glomeruli are innervated by trichoid ORNs thought to be selective for pheromones<sup>24</sup>. This innervation pattern (with slight variations) accounted for ~15% of all LNs in our data set from lines 1–7, notably those labeled by line 6 (**Fig. 3a**; see below), and 10% of cells we filled in electrophysiological recordings. These cells differed from other LNs in having especially transient bursts of excitation (**Fig. 5c,d**). Overall, this morphological class fired a higher percentage of their spikes in the first 100 ms of the response than did other LNs (**Fig. 5c**). Thus, these LNs could create a transient pulse of GABAergic inhibition at odor onset. If so, then some pheromone glomeruli would evidently be selectively excluded from this transient pulse of inhibition.

#### Line 6 LNs: coarse stereotypy and fine variability

Does the diversity we observed in LN morphology and physiology arise from variability of the same LNs across different individual flies, or from many diverse LN types each with stereotypic patterns in all individuals? The first alternative is implied by our finding of 847 distinct innervation patterns in 1,489 ipsilaterally projecting LNs (**Fig. 3a**), far

**Figure 5** Functional differences between morphological classes. **(a)** Pan-glomerular LNs ( $n = 26$ ) had significantly higher spontaneous activity ( $P < 0.01$ ) and weaker mean and maximum odor responses ( $P < 0.05$ ,  $t$ -tests) as compared to all other LNs that were successfully reconstructed ( $n = 67$ ). **(b)** Odor responses of three pan-glomerular LNs. **(c)** Left: pheromone-avoiding LNs ( $n = 9$ ) fired a significantly higher percentage of their spikes during the first 100 ms of the odor response as compared to all other LNs ( $n = 84$ ,  $P < 0.01$ ,  $t$ -test). (Because there is a delay of about 100 ms before odor actually reaches the fly, spikes were counted during the period 100–200 ms after nominal odor onset; this was divided by total spikes during the 1-s period shown in rasters.) Right: odor response time course was more transient for these LNs than for other LNs (mean peristimulus time histogram,  $\pm$  s.e.m. across cells). **(d)** Odor responses of three pheromone-avoiding LNs.

exceeding the estimated total number of ipsilaterally projecting LNs (~100) within an individual antennal lobe (Supplementary Table 1). LN arborization patterns therefore cannot be completely stereotyped across flies.

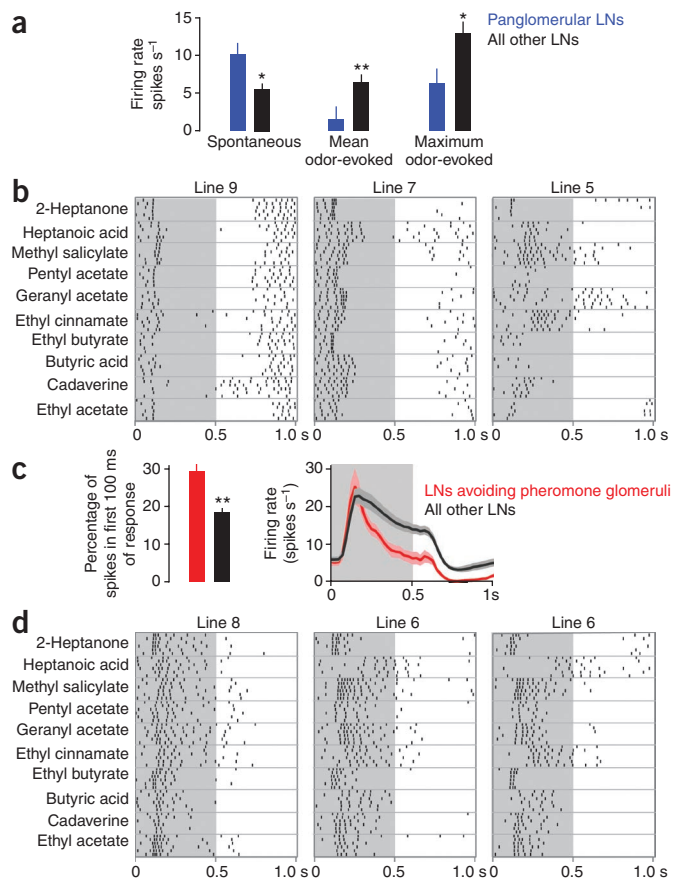
We sought to further address this question by dense sampling of a Gal4 line (line 6) that labeled a small population (seven LNs per antennal lobe; Supplementary Table 1). Among 131 labeled single cells for line 6, we observed 76 distinct glomerular innervation patterns (Fig. 6a). Because there were many more innervation patterns than the number of cells per fly, individual line 6-labeled LNs cannot be identical across flies.

Electrophysiological recordings showed that line 6 LNs also had diverse functional properties (Figs. 6b–e and 5c). Some cells (Fig. 6b,c) showed a transient burst at the onset of almost every odor, followed by inhibition. Other cells (Fig. 6d,e) showed sustained excitation and more odor-specific tuning. Thus, neither the morphology nor the physiology of line 6 LNs was highly stereotyped.

Despite the clear evidence that individual LNs labeled by line 6 were not rigidly stereotyped, the properties of these LNs were far from randomly distributed. For example, the odor response properties of line 6 cells were significantly less varied across cells than the odor response properties of all LNs. Mean and maximum odor-evoked firing rates were less variable within the line 6 population ( $n = 16$ ) than across the LN population as a whole ( $n = 92$ ,  $P < 5 \times 10^{-5}$ ,  $F$ -tests). In addition, spontaneous firing rates were also less variable within the line 6 population than across all LNs ( $P < 5 \times 10^{-6}$ ,  $F$ -test).

The glomerular innervation patterns of line 6 LNs were also far from random. Each line 6 LN innervated 51.1 glomeruli ( $n = 131$ , s.e.m. = 0.22) on average. If the innervation pattern were completely random, then every glomerulus would have a 94.4% probability of being innervated. Assuming a binomial probability distribution, the number of samples innervating a glomerulus should vary by the standard error,  $\pm 2\%$ . The actual distribution clearly deviates from this prediction (Fig. 6f). Most glomeruli were almost always innervated, whereas a subset of glomeruli were often missed. Among this latter group of glomeruli, VA1d was most often omitted. Indeed, most of the biocytin-filled LNs that selectively avoided VA1d (Fig. 5d) were line 6 LNs (7 of 9).

Because our binary scores for innervation patterns are only a coarse measure of a LN's morphology, we also measured the innervation density of line 6 LNs for selected glomeruli that were either always innervated or often missed. We found that DM1 (always innervated) has a significantly higher innervation density than VA1d or DA1 (occasionally innervated), whereas randomly selected pan-glomerular LNs showed similar innervation densities for DM1, VA1d and DA1. Innervation density of line 6 neurons in DA1 and VA1d glomeruli was significantly lower than that of pan-glomerular LNs (Fig. 6g). These



data strengthen the distinction of these two groups of glomeruli with regard to line 6 LN innervation. One group was always innervated, whereas the other group had much less innervation, when not being completely avoided.

In summary, analysis of line 6 indicated a principle likely applicable to most other morphologically and genetically defined classes of LNs. LNs showed marked variability within a class, and some of this variability must represent variations in the same cells across different brains. Yet the properties of these LNs are clearly not drawn randomly from the entire distribution of LN properties. This picture is consistent with the idea that the coarse properties of these cells are genetically preprogrammed, whereas their finer-scale properties may also reflect factors such as developmental plasticity and sensory experience.

#### Patchy LNs: a potential mechanism for variability

The variability of glomerular innervation patterns is exemplified in a small subset of LNs from lines 1, 3 and 5 that showed a distinctive pattern of patchy innervation (Figs. 2d and 3e). Remarkably, comparison of the glomerular innervation patterns of 161 patchy cells (Fig. 7a) indicated that none of these single cells innervated identical sets of glomeruli. Given that these patchy cells represent only a small fraction of cells labeled by each LN line and a small fraction of the ~100 ipsilaterally projecting LNs, it is clear that the innervation patterns of patchy LNs are highly variable across different individual flies.

The patchy nature of these cells' innervation patterns suggested that these innervation patterns might be established through cell-cell interactions among LNs. To examine the relationships between innervation patterns of different LNs in the same fly, we designed a genetic method to visualize a pair of sister patchy cells with two different

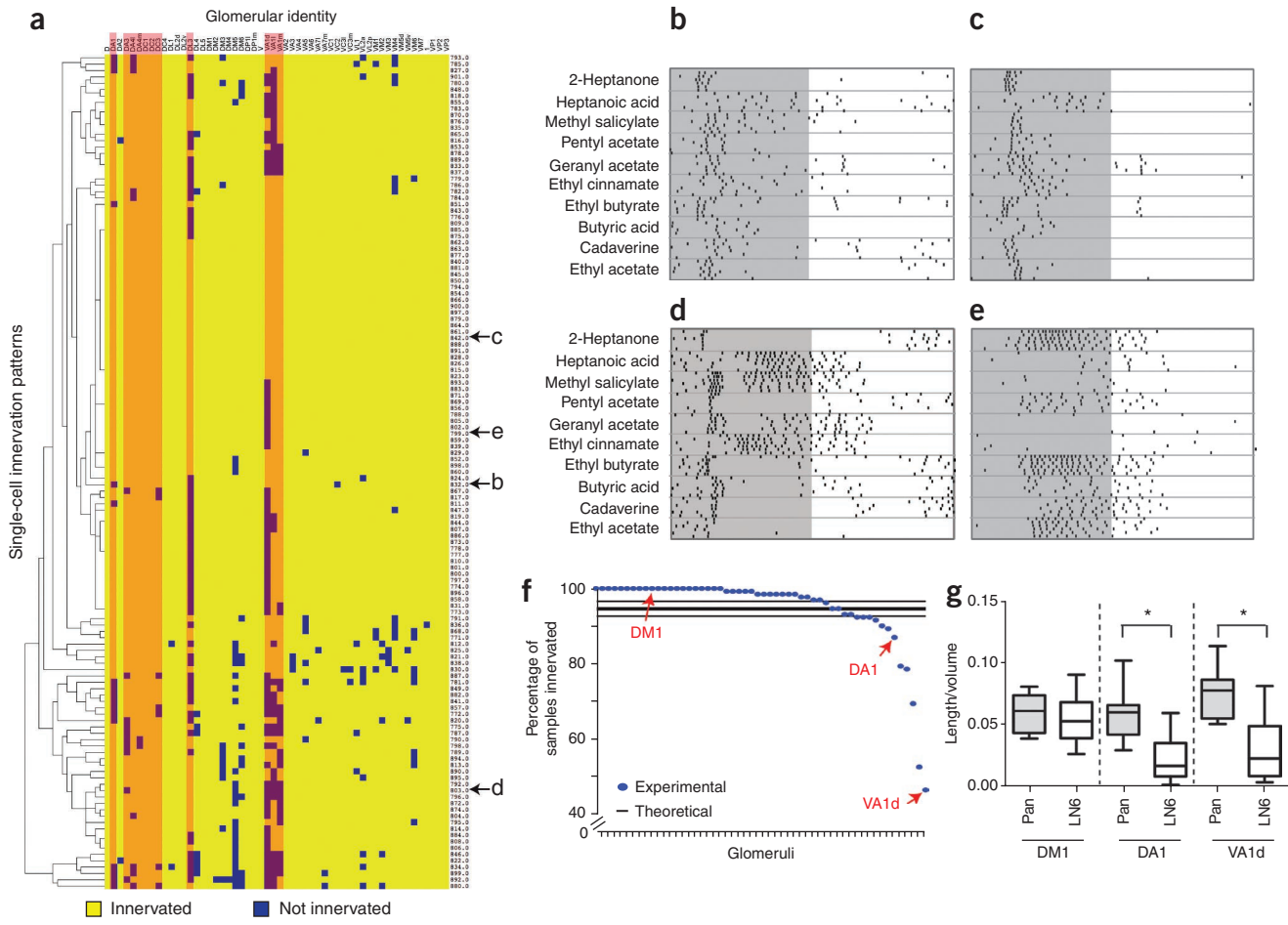


**Figure 6** Variability and stereotypy of line 6 LNs. **(a)** Hierarchical clustering of innervation patterns, as in **Figure 3a** but only for line 6 LNs ( $n = 131$ ). Cells in **b–e** are indicated. Glomeruli innervated by trichoid ORNs (pheromonal glomeruli) are highlighted in orange.  $k$ -means clustering verified that line 6 binary innervation patterns form a single cluster. Some cells were from flies in which antennae, maxillary palps or both had been removed for 10 d before fixation (**Fig. 8e,f**), but these treatments did not affect the number or the variability of glomerular innervation (**Supplementary Fig. 11**). **(b–e)** Odor response of four line 6 LNs. Shaded regions of plots denote odor stimulus period (500 ms). **(f)** Comparison of experimental (blue dots) and theoretical frequency of innervation if glomeruli were randomly innervated (center black line). The envelope of  $\pm 2\%$  is the standard error assuming a binomial distribution of innervation frequencies. In the experimental frequency, many glomeruli were almost always innervated, significantly above the theoretical distribution; other glomeruli were innervated significantly less frequently than the theoretical distribution. The glomerular identities to the right of DA1 are DM5, VA1m, VA1l, DL3 and VA1d; all except DM5 are pheromonal glomeruli. **(g)** Box plot quantification of innervation density of DM1, DA1 and VA1d from ten randomly chosen LNs of each class that innervated all three glomeruli. Center line denotes the average, the box encloses to the limits of the top and bottom quartiles and the whiskers extend to the maximum and minimum values. Innervation density = total dendritic length in glomerulus / glomerulus volume. Innervation of DA1 and VA1d by line 6 LNs (LN6) was significantly lower (Tukey's test,  $*P < 0.05$ ) than that of control LNs (panglomerular (pan) LNs randomly selected from lines 1, 3 and 5). Dotted lines separate measurements from different glomeruli.

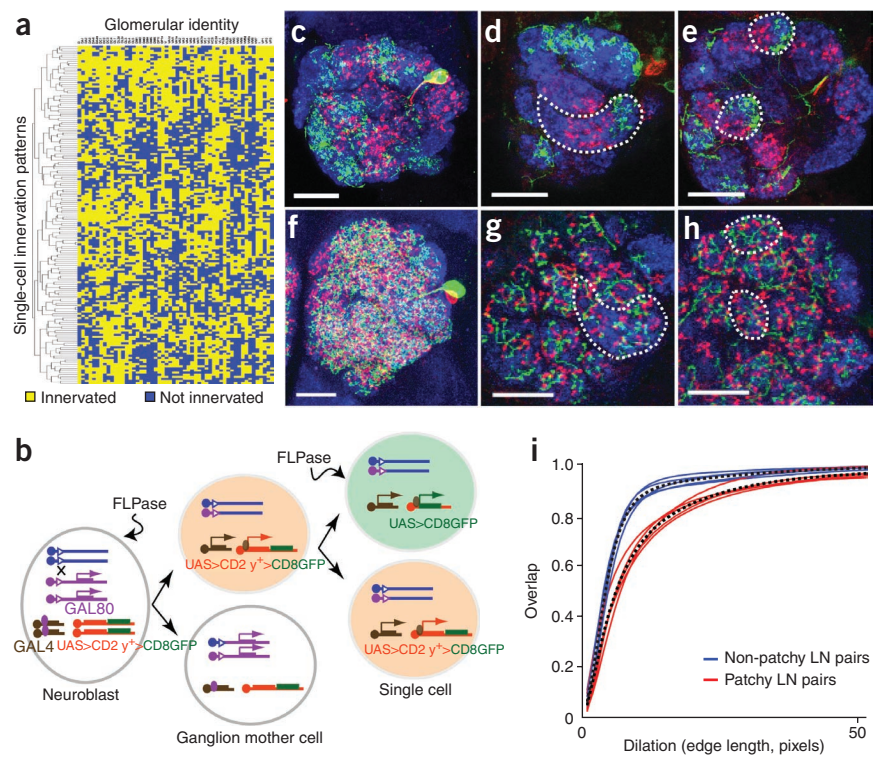
colors (**Fig. 7b**). Although the efficiency of this method was extremely low, yielding only five pairs of patchy cells among thousands of dissected brains, it is evident that processes of sister patchy cells avoided each other to carve out their innervation domains, sometimes by splitting a single glomerulus (outlined in **Fig. 7d,e** and **Supplementary Fig. 10**). By contrast, differentially labeled sister cells of other LN types intermixed at much finer scales (**Fig. 7f–h**). We confirmed the qualitative difference by quantifying the degree of overlap between the signals of the two cells after the signals had been systematically diluted to varying degrees (see Online Methods). Non-patchy cells showed a great deal of overlap with just a small amount of dilation, whereas patchy cells showed similar degrees of overlap only after their signals had been diluted much more (**Fig. 7i**). These observations suggest that sister patchy LNs may tile the antennal lobe the way ganglion cells tile the vertebrate retina<sup>27</sup> and sensory neurons tile the *Drosophila*

body wall<sup>28</sup>. We also estimated that each patchy LN occupied  $13.1 \pm 1.6\%$  (mean  $\pm$  s.d.,  $n = 8$ ) of the antennal lobe volume, implying that eight patchy LNs could tile an entire antennal lobe. These findings suggest that LN–LN interactions play a role in establishing patchy LN morphologies.

#### Development and maintenance of LN innervation patterns

Finally, we tested the contributions of ORNs to the glomerular arborization pattern of LNs. During the construction of the antennal lobe circuit, PN dendrites initiate pattern formation before the arrival of pioneering axons by targeting dendrites to positions similar to those where they are found in the adult antennal lobe. ORN axon invasion into the antennal lobe and subsequent ORN axon–PN dendrite recognition results in the formation of distinguishable glomeruli<sup>29,30</sup>. The development of LNs has not previously been described.

**Figure 7** Variability of patchy LNs. (a) Clustering of 161 patchy cell innervation patterns, as in Figure 3a. No two cells had identical innervation patterns. (b) Schematic of MARCM-FLP-out, which allows two sister cells to be labeled by different colors. *UAS-FRT-CD2-FRT-mCD8GFP* (ref. 40) serves as a reporter of Gal4. After FLP-mediated mitotic recombination causes the loss of Gal80 in the ganglion mother cell (GMC), CD2 (red) should be expressed in both daughter cells derived from this GMC. However, if an additional FLP-out event occurs in one of the two daughter cells, this cell will express mCD8-GFP (green) instead of CD2. (c–h) Examples of two sister patchy cells (c–e) and two sister control cells (f–h) labeled by MARCM-FLP-out, shown with N-cadherin (blue), GFP (green) and CD2 (red) staining. (c,f) Projection of the entire antennal lobe. (d,e,g,h) High magnification of 5- $\mu$ m projections from anterior (d,g) and middle (e,h) antennal lobe sections, showing nonoverlapping processes from two sister cells. Dashed lines, boundaries of glomeruli VA1/m (d) and DL1 and DC2 (e). Scale bars, 20  $\mu$ m. (i) Sister cell overlap index as a function of edge length of the dilation kernel (see Online Methods). Dashed lines indicate the mean for patchy sister cells (right-shifted) and non-patchy sister cells (left-shifted). Colored lines indicate individual pairs of sister cells. A quantitative distinction between patchy and non-patchy classes was verified by *k*-means clustering into two clusters.



We first tested whether LN arborization during pupal development required ORN axons (Fig. 8a–d). We made use of the facts that Hedgehog signaling is required for antennal disc proliferation, and clonal loss of Smoothened, a component essential for Hedgehog signaling, results in occasional loss of maxillary palps while leaving the antennae intact<sup>30</sup>. Under this condition, ORN axons from the antennae would innervate glomeruli that are normal targets of antennal ORN axons, but glomeruli that are normal targets of maxillary palp ORNs are devoid of ORN input<sup>30</sup>. By introducing line 5 Gal4-driven mCD8-GFP into this genetic background and examining flies with bilateral loss of maxillary palps (~1 in 250; Fig. 8a), we found that LN processes were not present in the glomeruli that are normal targets of maxillary palp ORNs. LN processes still innervated the nearby glomeruli that are targets of antennal ORNs (Fig. 8b, bottom panels, compared to Fig. 8b, top panels; Fig. 8d). By contrast, PN dendritic processes were mostly still present in glomeruli devoid of ORN axons (Fig. 8c,d). This experiment suggests that glomerular innervation of LNs requires the presence of ORN axons.

To test whether ORN axons are required for the maintenance of LN processes, we bilaterally removed the maxillary palps in adults, which is well after antennal lobe wiring is completed. We examined the processes of line 6 LNs (which are a subset of line 5 LNs examined in the previous experiment (Supplementary Table 1)) at least 10 d after removal of the maxillary palps to allow complete degeneration of ORN axons. We found that LN processes still innervated maxillary palp glomeruli (Fig. 8e). The volume of one of the two glomeruli quantified was significantly lower (Fig. 8f, top panel), likely because ORN axons contribute to the glomerular volume<sup>31</sup>. However, the total length of LN processes and the total number of presynaptic terminals as marked by synaptotagmin-HA puncta were unaffected by the adult removal of ORNs (Fig. 8f, middle and bottom panels). We also compared variability of glomerular innervation patterns of line 6 LNs between wild-type

flies and those with ORNs removed. We found no significant differences in either the number of glomeruli innervated or unique innervation patterns (Supplementary Fig. 11), suggesting that variability of line 6 LNs is not dependent on the presence of ORN axons in adult. Taken together, these experiments indicate that ORN axons are essential for LN innervation during development but are not required for the maintenance of their glomerular innervation in adulthood.

## DISCUSSION

Knowledge of local interneuron properties is essential to understand how a neural circuit processes information. Here we present a systematic single-cell analysis of >1,500 antennal lobe LNs in *Drosophila*. The scale of our analysis is an order of magnitude greater than that of the most comprehensive analysis of insect LNs yet published<sup>8</sup>. Our genetic strategy also avoided sampling biases involved with dye filling, which favors large cells with easy access. Despite the caveat that our sampling of LNs was not entirely even (see Online Methods), our study revealed a diversity of antennal lobe LNs beyond that described previously in any insect. LNs were diverse in their neurotransmitter types, glomerular innervation patterns, fine dendritic structures, densities and distribution of presynaptic terminals, and odor response properties. Furthermore, our analysis of glomerular innervation patterns and odor responses revealed coarse stereotypy but also an unexpected degree of fine-scale variability in genetically defined subclasses of LNs. Below we discuss the implications of these findings for the development and function of the antennal lobe circuit, and for the complexity of the *Drosophila* brain as a model for neural circuit analysis.

## How is the morphological diversity of LNs established?

The final glomerular innervation patterns of LNs likely result from some combination of (i) genetic specification, (ii) cell-cell interactions

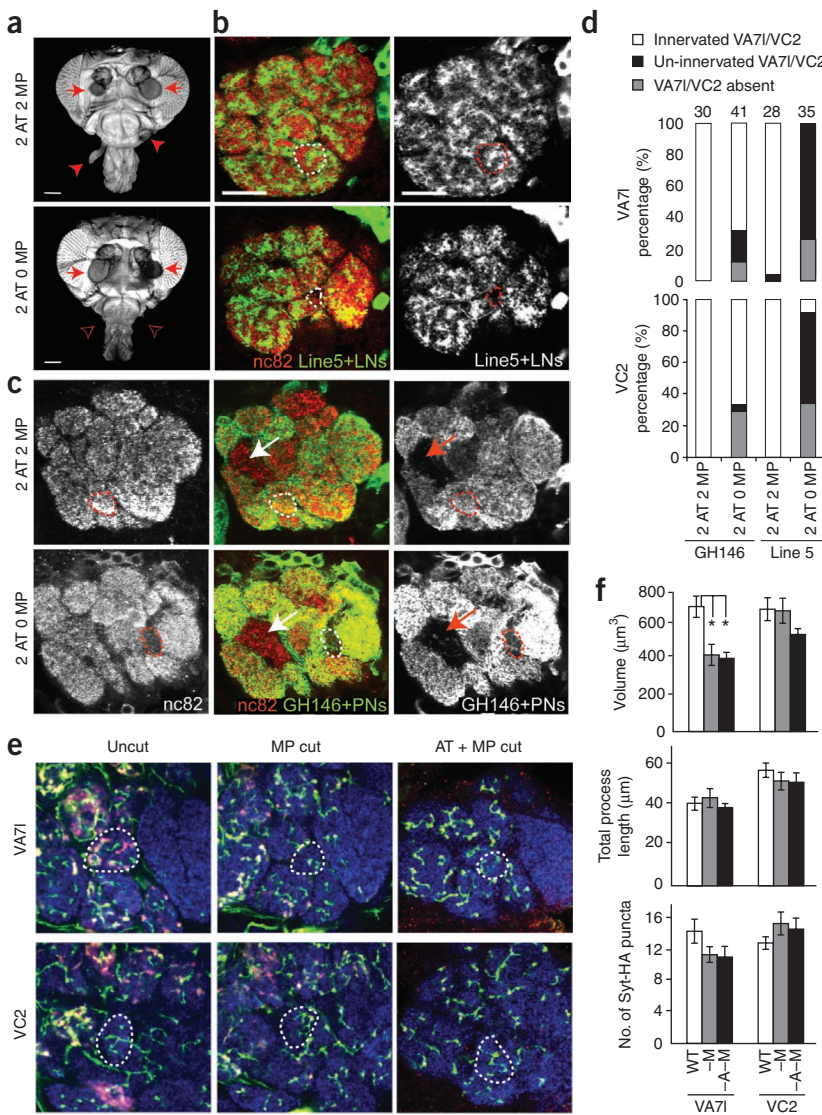


**Figure 8** Development but not maintenance of LN arborization depends on ORNs.

(a) Top: normal adult fly head with two antennae (2 AT, arrows) and two maxillary palps (MP, arrowheads). Bottom: occasionally, eyFLP-induced *smo* clones eliminate both MPs (open arrowheads). Scale bars, 100  $\mu$ m. (b,c) Brains from normal (top) and O-MP (bottom) flies carrying *Line5-Ga4* (b) or *GH146-Ga4* (c) labeled by nc82 and Gal4-driven mCD8GFP as indicated. The MP ORN target VA7I glomerulus (dotted circle) was not innervated by line 5 processes in O-MP flies but was still innervated by PN processes. Arrows designate glomeruli that are innervated by GH146-negative PNs. Scale bars, 20  $\mu$ m. (d) Quantification of glomerular innervation by *Line5-Ga4* LN and *GH146-Ga4* PN processes in the presence or absence of ORN innervation of MP target glomeruli VA7I (top) and VC2 (bottom). (e) Representative single sections of line 6 LN single-cell clones after adult removal of MPs or of both MPs and ATs. Control samples (uncut) show line 6 LN innervation of VA7I (top) and VC2 (bottom). After adult removal of MPs or of both MPs and ATs, line 6 LNs still innervated VA7I and VC2. Blue, nc82; green, mCD8-GFP; red, synaptotagmin (Syt)-HA. (f) Quantification of glomerular volume, LN process length and the number of Syt-HA puncta in control (WT), MP cut (-M) or MP and AT cut (-A-M) brains. The VA7I volume was significantly lower when ORN processes were removed, but neither process length nor the number of synaptotagmin-HA puncta in VA7I and VC2 was significantly reduced. Error bars, s.e.m.

by line 6. One may imagine that mechanisms that translate lineage and birth timing to wiring specificity of PNs and other glomerular targeting mechanisms<sup>32</sup> can also be used to specify glomerular innervation specificity of certain types of LNs.

Compared to ORNs and PNs, however, LN glomerular innervation patterns were much more variable and less deterministic. The most noteworthy example was patchy LNs: the 161 single cells we examined showed 161 distinct glomerular innervation patterns. Our two-cell clone analysis suggests a developmental mechanism for achieving this diversity. We found that processes of sister patchy cells tended to avoid each other even when they innervated common glomeruli. Our quantitative analysis is consistent with the idea that these complex dendrites tile the three-dimensional volume of the antennal lobe. These data suggest that homotypic repulsion might play a role in establishing final innervation patterns of some LN morphological types. From a functional perspective, it seems likely that the specific glomerular innervation patterns of individual patchy LNs are unimportant as long as a group of similar types of patchy LNs cover the entire antennal lobe.

### Functional implications

Local interneuron classes defined by morphology and molecular markers are thought to have distinct functions<sup>1</sup>. The *Drosophila* antennal lobe represents an unusual opportunity to assess *in vivo* the functional correlates of LN classes. Overall, we found that LNs varied widely in their odor-evoked firing rates and their temporal dynamics.

The selective modulation of LNs with particular dynamics could be a way to modulate the temporal pattern of PN activity.

On a coarse level, some physiological diversity correlated with differences in morphology or genetic markers. For example, pglomerular LNs had unusually high rates of spontaneous activity, suggesting that they may be particularly important in broadcasting tonic inhibition throughout the antennal lobe. Tonic inhibition is thought to regulate the sensitivity of odor detection in the mammalian olfactory bulb<sup>33,34</sup>. Pglomerular LNs either were inhibited by odors or were only weakly excited. Because they are mainly GABAergic, inhibition of pglomerular LNs would tend to disinhibit the entire antennal lobe in response to odors.

To take another example, LNs that avoid certain pheromone-selective glomeruli fired unusually transient bursts at odor onset. These LNs may have a special role in inhibiting the initial 100 ms of PN odor responses, when PN firing rates peak<sup>35</sup>. Some pheromone glomeruli are evidently excluded from this inhibition. This may be an adaptation to the relatively weak ORN firing rates elicited by pheromones<sup>24</sup> and may help explain why weak ORN responses to pheromones can be strongly amplified in postsynaptic PNs<sup>36</sup>.

Although we found a coarse correlation between some functional properties and morphological or genetic classifications, we also found that each LN class we examined in finer detail contained substantial diversity. For example, both pglomerular and pheromone-avoiding LNs had varied odor responses. Similarly, line 6 LNs were also heterogeneous, especially considering that there were only ~7 such cells. Thus, we are unlikely to be able to accurately predict every aspect of an LN's physiology on the basis solely of its morphology or a few molecular markers. Notably, interneurons of the mammalian cortex are also remarkably varied, prompting the remark that "inhibitory cells seem to be so diverse as perhaps to endanger the notion of cell types in the central nervous system"<sup>37</sup>. Here we have shown that interneuron diversity in the *Drosophila* brain rivals that of the mammalian brain, and we have begun to establish developmental principles underlying this diversity.

### Complexity of the *Drosophila* brain

It is widely believed that, compared to vertebrates<sup>38</sup>, invertebrate nervous systems are much more stereotyped across different members of the same species, with individually identifiable neurons and stereotyped connection patterns. Indeed, previous analysis of projection patterns of individual antennal lobe PNs provided a notable example in support of this notion<sup>39,40</sup>. Thus, the degree of variability of glomerular innervation patterns of individual LNs was unexpected. Such variability should translate into variability in the functional connectivity of LNs, ORNs and PNs.

Although the glomerular organization of the antennal lobe provides a convenient and unequivocal demonstration of variability in the *Drosophila* 'connectome', it remains to be determined whether variable connectivity is a general feature of the fly brain. Interestingly, even the axons of antennal lobe PNs, which showed notably stereotyped terminal arborization patterns in the lateral horn, show less stereotypy in the mushroom body<sup>23,39,40</sup>. Indeed, a recent physiology study suggests non-stereotypic connections between PN axons and their postsynaptic targets in the mushroom body<sup>41</sup>. It is possible that, upon detailed examination, such lack of stereotypy is the norm rather than an exception, even in the relatively simple insect brain.

We and others<sup>42</sup> believe that a wiring diagram is a necessary (although certainly not sufficient) prerequisite for understanding the function of neural circuits. However, our results imply that the complete reconstruction of the wiring diagram of a single *Drosophila*

brain will not yield a general wiring diagram for all *Drosophila* brains. At the same time, our findings identify a fundamental similarity between insect and vertebrate brains in the variability of their connectomes. Although it may prove more challenging than previously assumed to map the connectivity of the fly brain, solving the *Drosophila* connectome may turn out to be more relevant to understanding our own brain.

### METHODS

Methods and any associated references are available in the online version of the paper at <http://www.nature.com/natureneuroscience/>.

*Note: Supplementary information is available on the Nature Neuroscience website.*

### ACKNOWLEDGMENTS

We thank U. Heberlein (University of California, San Francisco) and E. Marin for respectively providing and screening unpublished Gal4 lines, which lead to identification of line 1 and line 6; J. Simpson (Janelia Farm, Howard Hughes Medical Institute) for providing unpublished LCCH3 (line 7) Gal4; K. Wehner (Stanford University) for mouse anti-HA; A. DiAntonio (Washington University) for rabbit anti-DVGLUT; and the Bloomington Stock Center, Kyoto Stock Center, Drosophila Genetic Resource Center, Gal4 Enhancer Trap Insertion Database (GETDB), and Developmental Studies Hybridoma Bank for other reagents.

M.L.S. is grateful for the help of J. Brooks in data collection. We thank the Stanford Department of Statistics Consulting Service for technical help with statistical analyses. We thank T. Clandinin, G. Jeffreys and members of the Luo and Wilson laboratories for helpful comments on the manuscript. This work was supported by US National Institutes of Health grants to L.L. (R01-DC005982) and R.I.W. (R01-DC008174), a Pew Scholar award, a McKnight Scholar award, a Sloan Foundation research fellowship, and a Beckman Young Investigator award (to R.I.W.). M.L.S. is supported by a US National Research Service predoctoral award. E.Y. is supported by a Human Frontiers Science Program Long Term Fellowship. J.C.S.L. is supported by the Medical Scientist Training Program at Stanford University. L.L. receives investigator support from the Howard Hughes Medical Institute.

### AUTHOR CONTRIBUTIONS

Y.-H.C. and M.L.S. performed the anatomical and developmental experiments. E.Y. performed the physiological experiments. J.C.S.L. helped with statistical analysis. L.L. and R.I.W. supervised the project and wrote the paper.

### COMPETING FINANCIAL INTERESTS

The authors declare no competing financial interests.

Published online at <http://www.nature.com/natureneuroscience/>. Reprints and permissions information is available online at <http://npg.nature.com/reprintsandpermissions/>.

1. Markram, H. *et al.* Interneurons of the neocortical inhibitory system. *Nat. Rev. Neurosci.* **5**, 793–807 (2004).
2. Olsen, S.R. & Wilson, R.I. Cracking neural circuits in a tiny brain: new approaches for understanding the neural circuitry of *Drosophila*. *Trends Neurosci.* **31**, 512–520 (2008).
3. Vosshall, L.B. & Stocker, R.F. Molecular architecture of smell and taste in *Drosophila*. *Annu. Rev. Neurosci.* **30**, 505–533 (2007).
4. Shepherd, G.M., Chen, W.R. & Greer, C.A. Olfactory Bulb. in *The synaptic Organization of the Brain* (ed. Shepherd, G.M.) (Oxford University Press, Oxford, 2004).
5. Lledo, P.M., Merkle, F.T. & Alvarez-Buylla, A. Origin and function of olfactory bulb interneuron diversity. *Trends Neurosci.* **31**, 392–400 (2008).
6. Wachowiak, M. & Shipley, M.T. Coding and synaptic processing of sensory information in the glomerular layer of the olfactory bulb. *Semin. Cell Dev. Biol.* **17**, 411–423 (2006).
7. Christensen, T.A., Waldrop, B.R., Harrow, I.D. & Hildebrand, J.G. Local interneurons and information processing in the olfactory glomeruli of the moth *Manduca sexta*. *J. Comp. Physiol. A* **173**, 385–399 (1993).
8. Seki, Y. & Kanazaki, R. Comprehensive morphological identification and GABA immunocytochemistry of antennal lobe local interneurons in *Bombyx mori*. *J. Comp. Neurol.* **506**, 93–107 (2008).
9. MacLeod, K. & Laurent, G. Distinct mechanisms for synchronization and temporal patterning of odor-encoding neural assemblies. *Science* **274**, 976–979 (1996).
10. Fontan, C., Sun, X.J. & Masson, C. Morphology and spatial distribution of bee antennal lobe interneurons responsive to odours. *Chem. Senses* **18**, 101–119 (1993).

11. Ernst, K.D. & Boeckh, J. A neuroanatomical study on the organization of the central antennal pathways in insects. III. Neuroanatomical characterization of physiologically defined response types of deutocerebral neurons in *Periplaneta americana*. *Cell Tissue Res.* **229**, 1–22 (1983).
12. Stocker, R.F., Lienhard, M.C., Borst, A. & Fischbach, K.F. Neuronal architecture of the antennal lobe in *Drosophila melanogaster*. *Cell Tissue Res.* **262**, 9–34 (1990).
13. Wilson, R.I. & Laurent, G. Role of GABAergic inhibition in shaping odor-evoked spatiotemporal patterns in the *Drosophila* antennal lobe. *J. Neurosci.* **25**, 9069–9079 (2005).
14. Shang, Y., Claridge-Chang, A., Sjulson, L., Pypaert, M. & Miesenbock, G. Excitatory local circuits and their implications for olfactory processing in the fly antennal lobe. *Cell* **128**, 601–612 (2007).
15. Ng, M. et al. Transmission of olfactory information between three populations of neurons in the antennal lobe of the fly. *Neuron* **36**, 463–474 (2002).
16. Lai, S.L., Awasaki, T., Ito, K. & Lee, T. Clonal analysis of *Drosophila* antennal lobe neurons: diverse neuronal architectures in the lateral neuroblast lineage. *Development* **135**, 2883–2893 (2008).
17. Das, A. et al. *Drosophila* olfactory local interneurons and projection neurons derive from a common neuroblast lineage specified by the empty spiracles gene. *Neural Dev.* **3**, 33 (2008).
18. Okada, R., Awasaki, T. & Ito, K. Gamma-aminobutyric acid (GABA)-mediated neural connections in the *Drosophila* antennal lobe. *J. Comp. Neurol.* **514**, 74–91 (2009).
19. Lee, T. & Luo, L. Mosaic analysis with a repressible cell marker for studies of gene function in neuronal morphogenesis. *Neuron* **22**, 451–461 (1999).
20. Olsen, S.R., Bhandawat, V. & Wilson, R.I. Excitatory interactions between olfactory processing channels in the *Drosophila* antennal lobe. *Neuron* **54**, 89–103 (2007).
21. Lee, T., Lee, A. & Luo, L. Development of the *Drosophila* mushroom bodies: sequential generation of three distinct types of neurons from a neuroblast. *Development* **126**, 4065–4076 (1999).
22. Jefferis, G.S.X.E., Marin, E.C., Stocker, R.F. & Luo, L. Target neuron prespecification in the olfactory map of *Drosophila*. *Nature* **414**, 204–208 (2001).
23. Jefferis, G.S. et al. Comprehensive maps of *Drosophila* higher olfactory centers: spatially segregated fruit and pheromone representation. *Cell* **128**, 1187–1203 (2007).
24. van der Goes van Naters, W. & Carlson, J.R. Receptors and neurons for fly odors in *Drosophila*. *Curr. Biol.* **17**, 606–612 (2007).
25. Hallem, E.A. & Carlson, J.R. Coding of odors by a receptor repertoire. *Cell* **125**, 143–160 (2006).
26. Sachse, S. et al. Activity-dependent plasticity in an olfactory circuit. *Neuron* **56**, 838–850 (2007).
27. Wassle, H., Peichl, L. & Boycott, B.B. Dendritic territories of cat retinal ganglion cells. *Nature* **292**, 344–345 (1981).
28. Grueber, W.B., Jan, L.Y. & Jan, Y.N. Tiling of the *Drosophila* epidermis by multidendritic sensory neurons. *Development* **129**, 2867–2878 (2002).
29. Jefferis, G.S. et al. Developmental origin of wiring specificity in the olfactory system of *Drosophila*. *Development* **131**, 117–130 (2004).
30. Sweeney, L.B. et al. Temporal target restriction of olfactory receptor neurons by Semaphorin-1a/PlexinA-mediated axon-axon interactions. *Neuron* **53**, 185–200 (2007).
31. Berdnik, D., Chihara, T., Couto, A. & Luo, L. Wiring stability of the adult *Drosophila* olfactory circuit after lesion. *J. Neurosci.* **26**, 3367–3376 (2006).
32. Luo, L. & Flanagan, J.G. Development of continuous and discrete neural maps. *Neuron* **56**, 284–300 (2007).
33. Pirez, N. & Wachowiak, M. In vivo modulation of sensory input to the olfactory bulb by tonic and activity-dependent presynaptic inhibition of receptor neurons. *J. Neurosci.* **28**, 6360–6371 (2008).
34. Shao, Z., Puche, A.C., Kiyokane, E., Szabo, G. & Shipley, M.T. Two GABAergic intraglomerular circuits differentially regulate tonic and phasic presynaptic inhibition of olfactory nerve terminals. *J. Neurophysiol.* **101**, 1988–2001 (2009).
35. Bhandawat, V., Olsen, S.R., Gouwens, N.W., Schlieff, M.L. & Wilson, R.I. Sensory processing in the *Drosophila* antennal lobe increases reliability and separability of ensemble odor representations. *Nat. Neurosci.* **10**, 1474–1482 (2007).
36. Schlieff, M.L. & Wilson, R.I. Olfactory processing and behavior downstream from highly selective receptor neurons. *Nat. Neurosci.* **10**, 623–630 (2007).
37. Miles, R. Perspectives: neurobiology. Diversity in inhibition. *Science* **287**, 244–246 (2000).
38. Lu, J., Tapia, J.C., White, O.L. & Lichtman, J.W. The interscutularis muscle connectome. *PLoS Biol.* **7**, e32 (2009).
39. Marin, E.C., Jefferis, G.S.X.E., Komiyama, T., Zhu, H. & Luo, L. Representation of the glomerular olfactory map in the *Drosophila* brain. *Cell* **109**, 243–255 (2002).
40. Wong, A.M., Wang, J.W. & Axel, R. Spatial representation of the glomerular map in the *Drosophila* protocerebrum. *Cell* **109**, 229–241 (2002).
41. Murthy, M., Fiete, I. & Laurent, G. Testing odor response stereotypy in the *Drosophila* mushroom body. *Neuron* **59**, 1009–1023 (2008).
42. Lichtman, J.W. & Sanes, J.R. Ome sweet ome: what can the genome tell us about the connectome? *Curr. Opin. Neurobiol.* **18**, 346–353 (2008).
43. Laissue, P.P. et al. Three-dimensional reconstruction of the antennal lobe in *Drosophila melanogaster*. *J. Comp. Neurol.* **405**, 543–552 (1999).

## ONLINE METHODS

**Gal4 lines.** Line 1 (HB4-93) and line 6 (HB8-145) were identified from an anatomical screen of an unpublished Gal4 library from U. Heberlein. Line 2 (NP6277) and line 5 (NP3056) were ordered from the NP Gal4 library<sup>44</sup> on the basis of our various unpublished screens. Line 7 (LCCH3) is an unpublished line from J. Simpson. Other lines have been described before for their expression in LNs or in other brain neurons: line 3 is H24 (ref. 45); line 4 is GH298 (ref. 46); line 8 is Nan-Gal4 (ref. 47); line 9 is krasavietz-Gal4 (ref. 48); and line 10 is OK107 (ref. 21).

**Single-cell collections.** Our 1,532 single cells from ten Gal4 lines were collected over the course of 2 years, so experimental conditions varied. MARCM analysis used female flies 0–14 d old except for lines 2, 3 and 10, where a subset of experiments were performed with male flies, and line 9, which used exclusively males. A subset of line 6 single-cell clones were collected after antennae and/or maxillary palps were removed, so these flies as well as their untreated controls were dissected between 10–20 d after eclosion. All electrophysiology experiments were performed using females 2–3-d-old. Flies were reared at 25 °C for MARCM experiments and at room temperature (22–25 °C) for physiology experiments.

The relative frequency of single cells in our collection does not necessarily reflect the fraction of these cells in a given fly because of our sampling bias with regard to Gal4 lines and heat-shock windows: the number of MARCM-labeled single cells is not proportional to the number of LNs in a given Gal4 line, and not all developmental windows were equally sampled.

**MARCM, immunostaining and image processing.** MARCM analysis was performed according to established protocols<sup>19</sup>. Briefly, MARCM-ready stocks were crossed, eggs collected for various lengths of time (ranging from 2–24 h) and samples heat-shocked at time points of interest during embryonic, larval and early pupal development. Heat shocks at middle and late pupal stages rarely induced LN clones in our early experiments and thus were not used further. Heat-shock time windows for all cells are listed in **Supplementary Table 2**. Adult brains were dissected, fixed and stained as described before<sup>22</sup>. After staining, brains were mounted in SlowFade Gold (Molecular Probes) and imaged on a Zeiss Meta-510 confocal. Images were processed using LSM software (Zeiss) and Image J (<http://rsbweb.nih.gov/ij/>). Further measurements, including glomerular volume, dendrite length and synaptotagmin-HA density (Figs. 6 and 8), were made in Imaris (Bitplane) and statistical analysis performed in Excel and Graphpad Prism 5.0 software. To determine the volume of the antennal lobe occupied by individual patchy cells, LSM software was used to trace the outline of the antennal lobe (marked by N-cadherin) or patchy cell processes (labeled by GFP or CD2) in each confocal section collected at 1-μm intervals. The volume was determined as the sum of areas from each 1-μm section. Cell counts were performed manually or with the aid of Imaris.

Primary antibodies used included rat anti-mCD8a (1:100, Invitrogen), chicken anti-GFP (1:1,000; Aves Labs), rabbit anti-GFP (1:1,000, Molecular Probes), mouse anti-nc82 (1:30, Developmental Studies Hybridoma Bank (DSHB)), mouse anti-rCD2 (1:100, OX34, Serotec), rat anti-N-cadherin (1:40, DN-EX no. 8, DSHB), mouse anti-HA (1:100, 12CA5, gift from K. Wehner), rabbit anti-HA (1:1,000, Abcam), rabbit anti-β-galactosidase (1:1,000, CAPPEL/MB Biomedicals), chicken anti-β-galactosidase (1:1,000, Abcam), mouse anti-choline acetyltransferase (1:100, ChAT4B1, DSHB), rabbit anti-GABA (1:200, Sigma), rabbit anti-vesicular glutamate transporter (DVGLUT; 1:500; gift from A. DiAntonio). Secondary antibodies from Molecular Probes (MP) or Jackson ImmunoResearch Laboratories (JIRL) and used at 1:500 include: Zenon mouse Cy5 (MP), goat anti-mouse Cy3 (JIRL), goat anti-rat Alexa 488 (MP), goat anti-rat Cy5 (JIRL), goat anti-rat Cy3 (JIRL), goat anti-rabbit Alexa 488 (MP), goat anti-rabbit Cy5 (JIRL), donkey anti-chicken FITC (JIRL) and donkey anti-chicken Cy3 (1:300, JIRL).

**Physiology.** Whole-cell patch-clamp recordings from LN somata were performed as previously described<sup>13</sup>. External saline contained (in mM) 103 NaCl, 3 KCl, 5 N-tris(hydroxymethyl) methyl-2-aminoethane-sulfonic acid, 8 trehalose, 10 glucose, 26 NaHCO<sub>3</sub>, 1 NaH<sub>2</sub>PO<sub>4</sub>, 1.5 CaCl<sub>2</sub> and 4 MgCl<sub>2</sub> (osmolarity adjusted to 270–275 mOsm). The saline was bubbled with 95% O<sub>2</sub>/5% CO<sub>2</sub> and reached a pH of 7.3. The internal patch-pipette solution contained (in mM) 140 potassium aspartate, 10 HEPES buffer, 4 Mg-ATP, 0.5 Na<sub>3</sub>-GTP, 1 EGTA, 1 KCl and

13 biocytin hydrazide. The pH of the internal solution was adjusted to 7.3 and the osmolarity was adjusted to ~265 mOsm. LN somata were targeted by means of the GFP signal under epifluorescence illumination in an Olympus BX51WI microscope with a ×40 water-immersion objective. Spontaneous firing rates were measured in cell-attached mode before whole-cell break-in. After break-in, a small amount of hyperpolarizing current was injected constantly to compensate for the seal conductance and thereby to return the cell to its native spontaneous firing rate<sup>49</sup>. Recordings were acquired with an A-M Systems Model 2400 amplifier in current clamp mode (10-MΩ headstage), low-pass filtered at 2 kHz and digitized at 10 kHz. One neuron was recorded per brain and the morphology of each cell was visualized *post hoc* with biocytin-streptavidin and nc82 histochemistry as described previously<sup>35</sup> using a Zeiss LSM 510 META confocal microscope.

The total number of LNs recorded in each Gal4 line (and the number whose biocytin fills were successfully reconstructed) was as follows: line 5, 55 recorded (51 reconstructed), line 6, 18 (17), line 7, 21 (11), line 8, 8 (5), line 9, 11 (8). In some of these cells, we did not complete the full set of physiological measurements, which is why the number of experiments cited in connection with some statistical tests is smaller than the number listed here. We emphasize that this distribution is not necessarily representative of the actual underlying distribution of these LNs. For example, we deliberately oversampled line 5 in an attempt to hit some of the unusual morphological types labeled by this line (including patchy, dumbbell and oligoglomerular LNs). Despite these attempts, we were not able to record from any of these particular morphological classes of LNs, either for technical reasons (for example, their somata may be unusually small, or they may express low levels of GFP) or potentially due to a low abundance of these morphological classes. Thus, a systematic comparison of all morphological and physiological categories was not possible. The physiological diversity we describe is therefore only a lower bound on the diversity of the LN population.

Odors (Sigma) were delivered with a custom olfactometer, as described previously<sup>35</sup>. All odors were diluted 1:100 (vol/vol) in paraffin oil, and the odor vial headspace was diluted tenfold in air before reaching the fly. We chose a panel of ten odors to maximize the chemical diversity of our stimuli, to maximize overlap with odors used in other studies of the same ORNs and to activate a wide variety of ORN types to varying degrees<sup>50</sup>. To construct the peristimulus time histograms in **Figure 5c**, spike times were binned in 50-ms counting windows that overlapped by 25 ms. Each odor was presented six times at intervals of 40–60 s, and those trials were then averaged to generate a peristimulus time histogram for that combination of odor and cell. Where the odor response of a cell is expressed as a single time-averaged firing rate, these rates were measured over a 1-s period beginning at odor onset and are expressed as a change in firing rate relative to the spontaneous firing rate of that cell. Analyses were performed in IgorPro and in MATLAB.

**Statistical analysis of glomerular innervation patterns.** Scoring data in clustering analyses were collected manually by examining individual planes of 1-μm z-stacks. We identified 54 antennal glomeruli (**Fig. 3b**) in the nc82 or N-cadherin channel. A glomerulus was considered innervated if any green-colored LN process entered the nc82- or N-cadherin-dense region of a glomerulus.

Hierarchical clustering of innervation data was performed using freely available Cluster (<http://bonsai.ims.u-tokyo.ac.jp/~mdheo/cluster/software.htm>) or R (<http://www.r-project.org/>) software. Data were clustered using complete linkage and a Euclidean distance measure in either program. Results were visualized as dendograms and heat maps using JavaTreeView (<http://jtreeview.sourceforge.net/>) or native R graphics facilities. Coherent clusters (those with approximately unbiased P-values >90% or >95%) were identified in R using bootstrap analysis available through the pvclust package with *n* iterations ≥ 5,000. Hierarchical clustering was verified by comparison to iterative *k*-means-based clustering. We determined *k* for each iteration by plotting the within-groups sum of squares or by using the GAP statistic. Clusters identified by hierarchical clustering that correlated with those revealed by iterative *k*-means-based clustering were judged significant.

Innervation data were also imported into Matlab R2007a (Mathworks), where principal component analysis was performed using customized software. Data were centered by subtracting column means but were not rescaled.

Theoretical probabilities for LN6 innervation were calculated on the basis of the assumption that all glomeruli have an equal chance of being innervated.

Thus, for a given set of  $n$  innervation patterns, chance a given glomerulus is innervated = (total number of innervated glomeruli in the data set / 54) /  $n$ . Assuming that the collection of innervation probabilities is binomially distributed, the variation in observations can be calculated as s.e.m. =  $[p(1 - p) / n]^{1/2}$ , where  $p$  is the probability of innervation and  $n$  is the number of samples. These theoretical probabilities are presented in **Figure 6f** as the average percentage innervation by glomerulus,  $\pm$  s.e.m. as the upper and lower bounds.

We used the following intuition to quantify the overlap between patchy and non-patchy sister cells. For non-patchy sister cells colored red and green, a given volume of the antennal lobe of small size should contain both red and green signal, whereas for patchy sister cells, the same volume of antennal lobe could conceivably contain just red or just green signal. Only if the volume of interest were much larger should the strength of the overall red and green signals within the volume of interest become more comparable. To test this idea, we first excluded from the analysis cell bodies and brain regions outside the antennal lobe. An intensity threshold was then applied to sister cell image stacks to isolate the innervation patterns from background, with all pixels below the 97.5th percentile set to 0. Such thresholded images were then dilated using cube-shaped kernels of varying size. For image vectors  $\vec{r}$  and  $\vec{g}$ , an index of overlap OI was computed as follows:

$$OI(\vec{r}, \vec{g}) = \frac{\sum_{x,y,z} \vec{r}(x,y,z) \cdot \vec{g}(x,y,z)}{\|\vec{r}\| \cdot \|\vec{g}\|} = \cos(\theta)$$

using the Euclidean norm and where  $\theta$  is the angle between  $\vec{r}$  and  $\vec{g}$ . Finally, we plotted the overlap index as a function of dilation kernel size.

**Perturbation experiments.** To eliminate both maxillary palps in early development, *smo*<sup>3</sup> mutant clones were induced by eyFLP in flies expressing line 5

or GH146-Gal4–driven mCD8-GFP. Adults missing both MPs but retaining both antennae were dissected and their brains were analyzed for LN or PN innervation in glomeruli targeted by MP ORNs.

To remove ORN input in adults, MARCM-ready line 6 flies were heat-shocked between 24 and 72 h after egg-laying to generate single-cell LN clones. We severed and removed antennae, maxillary palps or both 0–2 d after eclosion using a Dumont no. 5 forceps. Flies were aged between 10 and 20 d before dissection and immunohistochemistry. Confocal images were loaded into Imaris, where individual glomeruli were traced to obtain volumetric measurements. LN projection length within individual glomeruli as well as Syt-HA puncta were also quantified using Imaris.

**Data access.** All the raw data used for clustering, including the confocal stacks of all LNs in **Supplementary Tables 2** and **3**, are accessible at <http://flybrain.stanford.edu/>.

44. Hayashi, S. *et al.* GETDB, a database compiling expression patterns and molecular locations of a collection of Gal4 enhancer traps. *Genesis* **34**, 58–61 (2002).
45. Martin, J.R., Ernst, R. & Heisenberg, M. Mushroom bodies suppress locomotor activity in *Drosophila melanogaster*. *Learn. Mem.* **5**, 179–191 (1998).
46. Stocker, R.F., Heimbeck, G., Gendre, N. & de Belle, J.S. Neuroblast ablation in *Drosophila* P[GAL4] lines reveals origins of olfactory interneurons. *J. Neurobiol.* **32**, 443–456 (1997).
47. Kim, J. *et al.* A TRPV family ion channel required for hearing in *Drosophila*. *Nature* **424**, 81–84 (2003).
48. Dubnau, J. *et al.* The staufen/pumilio pathway is involved in *Drosophila* long-term memory. *Curr. Biol.* **13**, 286–296 (2003).
49. Gouwens, N.W. & Wilson, R.I. Signal propagation in *Drosophila* central neurons. *J. Neurosci.* **29**, 6239–6249 (2009).
50. Hallem, E.A., Ho, M.G. & Carlson, J.R. The molecular basis of odor coding in the *Drosophila* antenna. *Cell* **117**, 965–979 (2004).